Coarsening model of cavity nucleation and thin film delamination from single-crystal $BaTiO_3$ with proton implantation

Jung-Wuk Hong, Jae-Ho Pyeon, and Joseph W. Tedesco
Department of Civil and Coastal Engineering, University of Florida, Gainesville, Florida 32611, USA

Young-Bae Park*
Thomas J. Watson Laboratories of Applied Physics, California Institute of Technology, Pasadena, California 91125, USA
(Received 9 November 2006; revised manuscript received 22 February 2007; published 5 June 2007)

The layer splitting mechanism of a proton implanted single crystal ferroelectric $BaTiO_3$ thin film layer from its bulk $BaTiO_3$ substrate has been investigated. The single crystal $BaTiO_3$ thin film layer splits as the hydrogen gas diffuses and the internal cavity pressure increases. Ripening mechanism driven by the pressurized hydrogen in the implantation-induced damage zone makes coarsening of the cavities and causes the delamination of the thin layer during the annealing. A unique criterion relation of blister nucleation and evolution has been derived and a simplified debonding criterion is proposed in terms of dimensionless parameters based on the force equilibrium condition. A numerical simulation of two-bubble evolution and delamination of thin film is performed using a finite element method.

DOI: 10.1103/PhysRevB.75.214102 PACS number(s): 62.20.Mk, 31.15.Qg, 62.30.+d, 81.40.Jj

Ion-implantation is a well established technique for surface modification, dopant injection, and device isolation in microelectronic device fabrication.[1] Because ion implantation is not constrained by the thermodynamic equilibrium of the host matrix, one can achieve supersaturated ion concentrations. The implantation energy and dose can be selected to precisely controlling the resulting ion depth distribution and damage concentration.

During the last decade, ion implantation-induced layer transfer processes have been reported for silicon, InP, GaAs, Ge, diamond, $LiNbO_3$, $SrTiO_3$, and $BaTiO_3$ in the microelectromechanical system (MEMS), optoelectronic, and electronic device fabrication.[2–8] Recently, silicon-on-insulator (SOI) substrate fabrication based on ion implantation and layer splitting techniques has been commercialized.[2] Wafer bonding and layer transfer techniques may someday become the preferred approach for generalized monolithic materials integration because of the versatility of the method for a variety of materials and the potential to reuse layer donor wafers many times for expensive materials.

The potential importance of layer exfoliation for advanced substrate technologies has encouraged researchers to devote study to the underlying mechanisms responsible for hydrogen induced blistering and layer delamination in order to elucidate the role of hydrogen in its interaction with the host material. Tong *et al.* and others have observed the formation of microbubbles and platelets in the region of the projected ion range in silicon and suggest that hydrogen diffusion is dominated by the lattice bonding structure.[9–11] Weldon and Bedell *et al.* have examined the layer splitting mechanism in proton implanted Si using spectroscopic technique such as nuclear resonance analysis (NRA) and Fourier transform infrared spectroscopy (FT-IR).[12,13] To date, the details of the cavity nucleation and growth mechanisms responsible for layer splitting have not been reported for ferroelectric materials. Even in silicon, there are few studies presenting a rigorous continuum mechanics approach[16] to the microbubble nucleation and growth mechanisms active in ion-implantation layer transfer processes.

Delamination of a thin film from a substrate has been extensively investigated in the field of continuum mechanics theory on various delaminating geometries such as "circular" and "random wrinkle."[14,15] However, the mechanical behavior and properties of delaminated and fractured thin films exfoliated from original donor materials through ion implantation have been rarely investigated.

In our previous study, we have identified hydrogen-induced blistering conditions for ferroelectric materials considering hydrogen diffusion and strain/stress build up during cavity nucleation and growth. We additionally found a critical cavity size based on thermodynamic considerations and studied cavity growth and exfoliation by atomic force microscopy and nanoindentation techniques.[17] In this paper, we have simulated the cavity growth and layer splitting phenomena using a finite element method (FEM) in conjunction with a unique force equilibrium criterion model.

Samples were prepared for this study by H^+ ion implantation into a bulk single crystal $BaTiO_3$ donor substrate (double side polished, (001)-orientation 10 mm $\times$ 10 mm $\times$ 1 mm). The implantation was performed at 25 °C to prevent blistering during the implantation and also to prevent any possible phase transition in the $BaTiO_3$ occurring at the Curie temperature of 125 °C.[8] The ion implantation energy was 80 keV for H^+ with a dose of 5×10^{16}–1×10^{17} cm^2. Simulation using the SRIM code suggests that this implantation results in an excess concentration of H^+ ions at a range of 500 nm. For the cavity nucleation and blistering observations, annealing was performed in a high vacuum ($<1\times10^{-6}$ torr) rapid thermal annealing (HV-RTA) chamber at temperatures ranging from 300 to 600 °C. We are able to exfoliate $BaTiO_3$ thin films with 500 nm thickness using this technique. These thin films show single crystal quality as in the original donor substrate.[8] The root mean square (rms) of surface roughness is in the few nm range because of the precise range of the implanted ions.

Polarized optical microscopy (POM), contact mode atomic force microscopy (AFM), and focused ion beam SEM

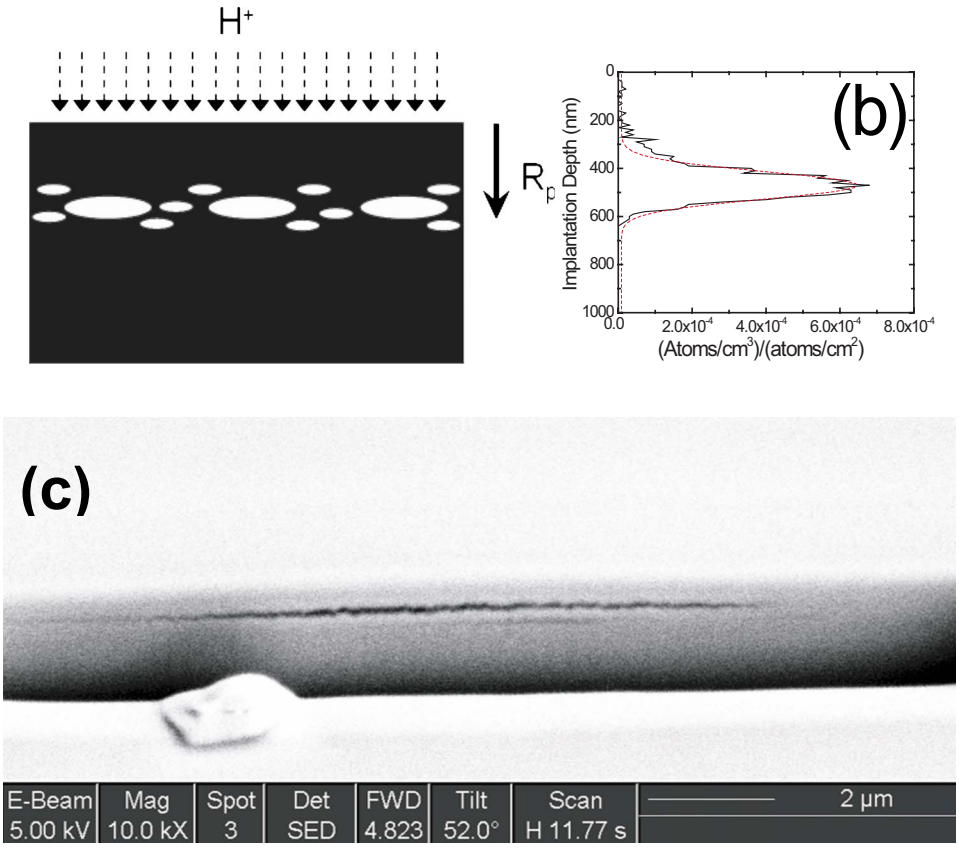

FIG. 1. (Color online) (a) A schematic diagram of bubble nucleation, (b) ion projected range of 80 keV protons implated into $BaTiO_3$ obtained by SRIM calculation. Data obtained from SRIM Monte Carlo simulation are fitted by Gaussian profiles to show the distribution of ions. (c) FIB-SEM image for a blister with post annealing at 400 °C.

(FIB-SEM) were used to take images of the cavity geometry and distributions. Forward recoil elastic spectroscopy (FRES) and temperature-programmed desorption spectroscopy (TDS) were used to study hydrogen behavior. Detailed results of these experiments will be shown elsewhere. Nanomechanical characterization of annealed $BaTiO_3$ samples was performed using a nanoindentation system in conjunction with an AFM.[17] Finite element method (FEM) simulation was performed with a commercially available code (LS-dyna).

In our system, hydrogen-induced blistering can be described as a three-step process. Atomic hydrogen is introduced into the donor via ion implantation as shown in Fig. 1(a). This phenomenon has been studied in metals, where it is referred to as internal hydrogen embrittlement (IHE).[19] After implantation, protons reside in the crystal lattice as hydrogen atoms at the depth of the projected ion range or might possibly be combined with other elements in the $BaTiO_3$ lattice. Atomic hydrogen diffuses through the lattice of donor, increasing the concentration in the tensile-stressed surroundings of a crack tip near the peak implantation region as shown in Fig. 1(b).[20] Diffusion is driven by a gradient in the chemical potential during high temperature annealing. As thermal annealing continues, the trapped hydrogen atoms begin to segregate, forming microcavities filled with pressurized H_2 molecules. The high pressure inside the cavity provides the driving force for growth and expansion during the initial stages of annealing.[16] Finally, the combined action of stress and hydrogen concentration leads to lateral crack propagation within the donor crystal. A FIB-SEM image in Fig. 1(c) shows the depth of ion projection and the local deflection of a thin delaminate.

In Figs. 2(a)–2(d), optical microscope images show typical cavity nucleation and growth after ion implantation and annealing According to fracture mechanics and thermodynamic nucleation theory, the shape and size of the cavity is determined by the number of gas molecules present and the surface energy and elastic parameters of $BaTiO_3$ at the annealing temperature. The maximum stable cavity size is predicted to be proportional to the annealing time at a temperature, in good agreement with our experimental results. The maximum cavity radius before rupture ranges from 1 to 10 μm depending on the annealing time and thermoelastic properties of the $BaTiO_3$. The detail discussion will be shown in another study. Regarding classical gas diffusion model assuming the first order diffusion, $\frac{\partial \phi_e(t,T)}{\partial t} = -k\phi_e(t,T)$ and ideal gas law, Han *et al.* showed kinetic mode of the cavity growth in hydrogen implanted Si and we also obtained similar trend in the hydrogen implanted $BaTiO_3$.[21] The exact solution of this kinetics model is shown in Fig. 2 caption and detail description will be published elsewhere.

By adopting Han's kinetic model for the $BaTiO_3$, a time-dependent cavity radius change is shown in Fig. 2(e). It shows an initial rapid increase of a single cavity's radius and above the saturation point a cavity is blistered and ruptured in the edge region of cavity as shown in Fig. 2(d). Circle symbol shows experimental result for 500 °C annealing. Error bars show the standard deviation and detection limit of minimum bubble sizes using optical microscope is ~1 μm. At short time region, cavity radius are scattered more due to the wide range of cavity radius. During cavity coalescence, nucleation and growth are governed by the energy minimi-

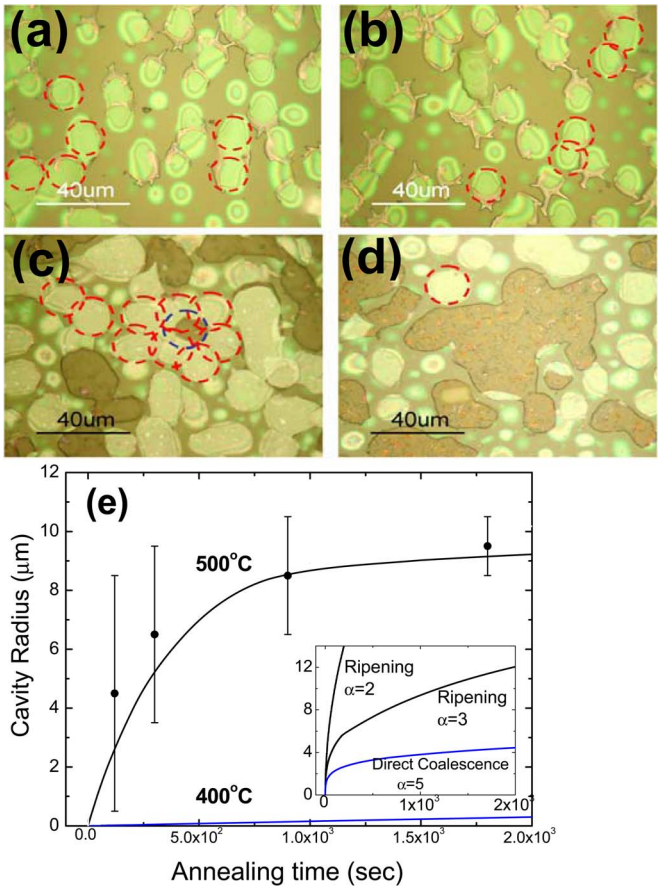

FIG. 2. (Color online) Time-dependent cavity evolution images (a) $t=120$ sec, (b) 300 sec, (c) 900 sec, and (d) 1800 sec obtained by optical microscope and focused ion beam-SEM image for a cavity. Circles in (a)–(d) represent the critical size for rupturing at the annealing temperature (500 °C). Anneal was under high vacuum (5×10^{-6} torr). (e) Kinetics calculation result considering hydrogen molecule diffusion kinetics. Parameters used are $k=1/\tau\exp[-(E_a+E_b)/kT]$ where $(E_a+E_b)=2.4$ eV obtained from FRES measurement (0.6 eV) and Ba-H (1.8 eV) bond energy. The governing equation of cavity growth is $r(t,T,\phi_o)=\frac{3\pi E\phi_o[1-\exp(-kt)]k_BT}{16(1-\nu^2)p^2}$ as derived in Ref. 21 where E is the Young's modulus, ϕ_0 is the ion dose, ν is the Poisson ratio, k_B is the Boltzmann constant, p is the cavity pressure, and T is the temperature.

zation of the entire system. Ortiz *et al.* have reported similar experiments on hydrogen behavior in metals.[22] In another earlier work, Chandrasekhar reported observations of both ripening and direct coalescence mechanisms.[23] Direct coalescence occurs when two voids join to form a larger void. The direct interaction can be imagined as a collision mechanism considering the diffusion or migration of individual cavities within the donor crystal. The ripening mechanism refers to the growth of large voids and the consumption of small via the Ostwald ripening process. In this work we consider both direct coalescence and Ostwald ripening as growth processes for an individual cavity. The cavity radius is related phenomenologically to the annealing time by $r\sim ct^{1/\alpha}$, where α depends on the underlying mechanism. In particular, $\alpha=5$ models direct coalescence while $\alpha=2-3$ is used for the ripening mechanism. In this study, we observed exponent value for the Ostwald ripening between 2 and 3 as shown in Fig. 2(e). Thus, we believed that the dominant interaction among cavities is therefore the Ostwald ripening process at the considering temperature range in this study in which cavity coalescence is governed by a long range interaction among the growing cavities. As shown in Fig. 2(e), however, direct coalescence also happens at a longer annealing time region. So, overall delamination process is a combination of direct coalescence and the Ostwald ripening processes.

Several researchers have previously investigated peeling phenomena and many different cohesive zone models have been proposed to explain debonding for a thin film on an elastic, or elastic-plastic substrate.[24,25] However, layer splitting in $BaTiO_3$ shows more complicated behavior, especially when a large number of bubbles are randomly generated by gas molecules introduced by ion implantation and the bubbles interact with each other. When the occupation ratio of blistered area over the total area is small, the evolution occurs in a steady manner. However, over a certain limit the thin film yields abruptly and delaminates from the donor substrate, possibly due to a weakened interfacial bonding strength caused by defects generated during high dose ion implantation. From a mathematical viewpoint, the moment of abrupt delamination from the substrate can be treated as a stability problem.

Here, we propose a simplified formulation from empirical observations considering parameters such as the area, pressure, and geometry of the bubbles and the bonding strength and material properties of the donor crystal. As shown in Fig. 3(b), let Ω_i be the area of each bubble $(\Omega_1,\ldots,\Omega_n)$, $\cup_i\Omega_i$ is the union of all debonded areas, and Ω is the entire domain. Applying force equilibrium condition in the vertical direction, we have the relation

$$\zeta(\Omega,\cup_i\Omega_i p_i,\sigma_b)=\sigma_b(\Omega-\cup_i\Omega_i)-\cup_i\Omega_i p_i\leqslant 0 \qquad (1)$$

where σ_b is the bonding stress criterion $(=\sqrt{2}\sigma_n)$, σ_n being the bonding stress in the normal direction, and p_i is the pressure in the ith blister. In Eq. (1), when $\zeta<0$, the thin film continues to evolve in a stable configuration. Each bubble grows in through the ripening and coalescence mechanisms. However, when the equilibrium condition, $\zeta=0$, is reached, the entire area delaminates in a sudden manner.

To formulate a simplified equation, we need to introduce an experimental-observation-based model of how $\cup_i\Omega_i$ depends on the pressure, bonding strength, elastic material properties of $BaTiO_3$ layer, and bubble geometries. A linear elastic material assumption allows us to separate the material related terms and geometry related terms as

$$\frac{\cup_i\Omega_i}{\Omega}=f\left(\frac{p}{\sigma_b},\frac{E}{\sigma_b},\nu\right)\tilde{K}(h,L,\ldots), \qquad (2)$$

where E is the Young's modulus, υ is the Poisson's ratio, h is the thickness of delaminated thin layer, L is the width of the material, the function f consists of nondimensional parameters describing material properties, and the function $\tilde{K}$ is related to bubble geometry and Poisson's ratio. As a simplest case, we take

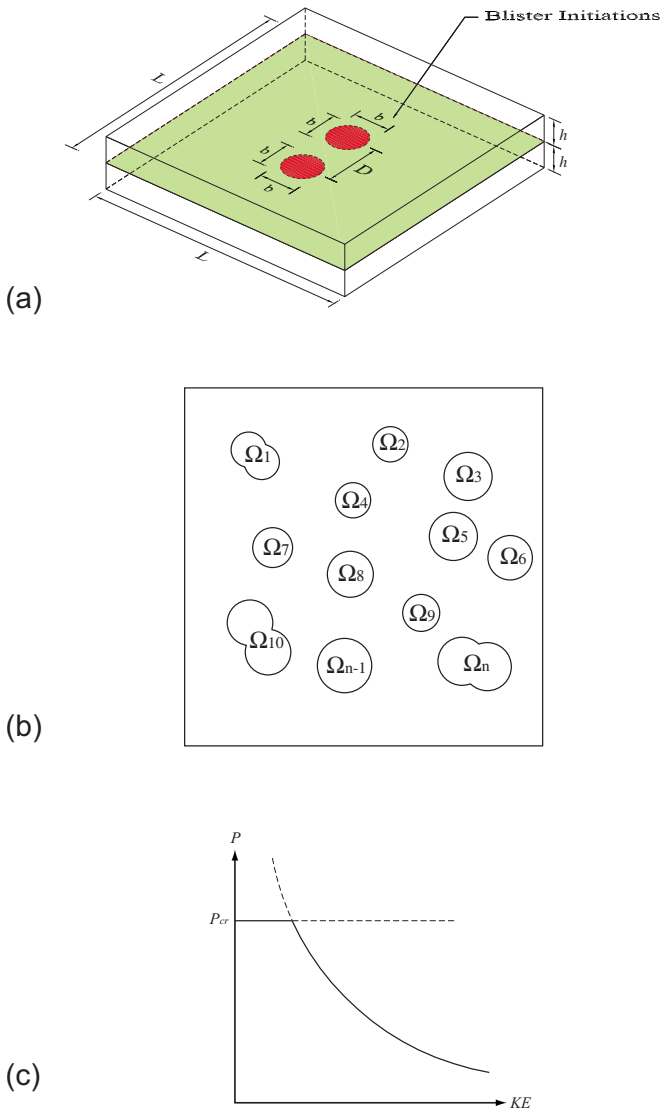

FIG. 3. (Color online) (a) A three-dimensional FEM model used to study blister evolution. Nucleation and growth of the blister are modeled with square debonded areas which have the radius b. The thickness of $BaTiO_3$ layer is h, the separation distance of blisters is D, and the width of layers is L. (b) An example of an initial bubble distribution in the substrate plate and (c) debonding criterion for a fixed value of σ_b.

$$\bigcup_i \Omega_i = K\frac{pE\Omega}{\sigma_b^2}, \tag{3}$$

where the variable K is a constant for a given geometry that is calculated from our experimental results. Equation (3) implies that propagation of the debonding area is related simply to the stiffness of the thin film and the bonding strength. The more flexible the thin film, the more internal pressure will be accommodated by strain rather than converted into debonding energy. Therefore, more pressure is required to complete the peeling of a thin film layer when the material is compliant. Substituting Eq. (3) into Eq. (1), we arrive at a simple polynomial equation

$$K\Omega p^2 + K\sigma_b\Omega p - \frac{\sigma_b^3\Omega}{E} \geqslant 0. \tag{4}$$

The solution of the Eq. (4) is

$$p = \frac{\sigma_b}{2}\left(\sqrt{1+\frac{4\sigma_b}{KE}} - 1\right), \tag{5}$$

when the value of (KE/σ_b) is very small [e.g. $(KE/\sigma_b) \approx 0$]. Equation (5) has a singularity. However it is possible to find an upper bound for the value of p according to Eq. (5) by solving Eq. (1) directly as

$$p_{cr} = \sigma_b\left(\frac{\Omega}{\bigcup_i \Omega_i} - 1\right). \tag{6}$$

The combination of Eq. (5) and Eq. (6) is illustrated in Fig. 3(c). Equation (6) shows that the critical pressure depends on the relative area damaged by ion implantation and the relationship between the bonding strength at the damage layer and Young's modulus for crystal, which describes the ability of the lattice to accommodate strain prior to film delamination.

As represented in Fig. 3, the thin $BaTiO_3$ layer to be delaminated from the top of the donor substrate is defined by an initial bonding interface created through ion implantation. This interface initially has several debonded areas that are considered as initiation sites for blisters. From the blister experiment shown in Fig. 2 and from AFM/nanoindentation characterization, the thickness (h) of the delaminating layer is 0.50 μm, and the interdistance (D) of bubbles is found to be 16 μm. The initial diameter (b) of blisters is 4.0 μm. The material properties are assumed to be linear elastic, with Young's modulus for the layers taken to be 120.0 GPa, and Poisson's ratio (υ) is assumed to be 0.3.[17]

Three-dimensional 8-node brick elements are adopted for the both top and bottom layers for FEM simulation. All the nodes at the bottom layer representing the donor wafer are held at fixed positions. Since we assume that the material property is linear elastic, rupture of the bubbles must be handled as a special case in the simulation. To model the initial interfacial debonding phenomenon, the bonding criterion is modeled with the relation[18]

$$\left[\frac{|\sigma_n|}{\hat{\sigma}_n}\right]^2 + \left[\frac{|\sigma_t|}{\hat{\sigma}_t}\right]^2 \geqslant 1, \tag{7}$$

where σ_n is the normal tensile stress, σ_t is the tangential shear stress, $\hat{\sigma}_n$ is the tensile failure stress, and $\hat{\sigma}_t$ is the shear failure stress. The stress value at each Gauss point is evaluated and the bonded contact condition is removed if Eq. (7) is satisfied, allowing the elements of the top layer to translate. At the bottom of the $BaTiO_3$ donor substrate layer, pressure increasing linearly in time is imposed up to a maximum of 200 MPa, as calculated using bubble geometry.[17]

As the internal pressure of a cavity increases, both cavity growth and debonding at the interface occur. As shown in Fig. 4(a), the volume of two individual cavities increases without significant debonding along the interface at low

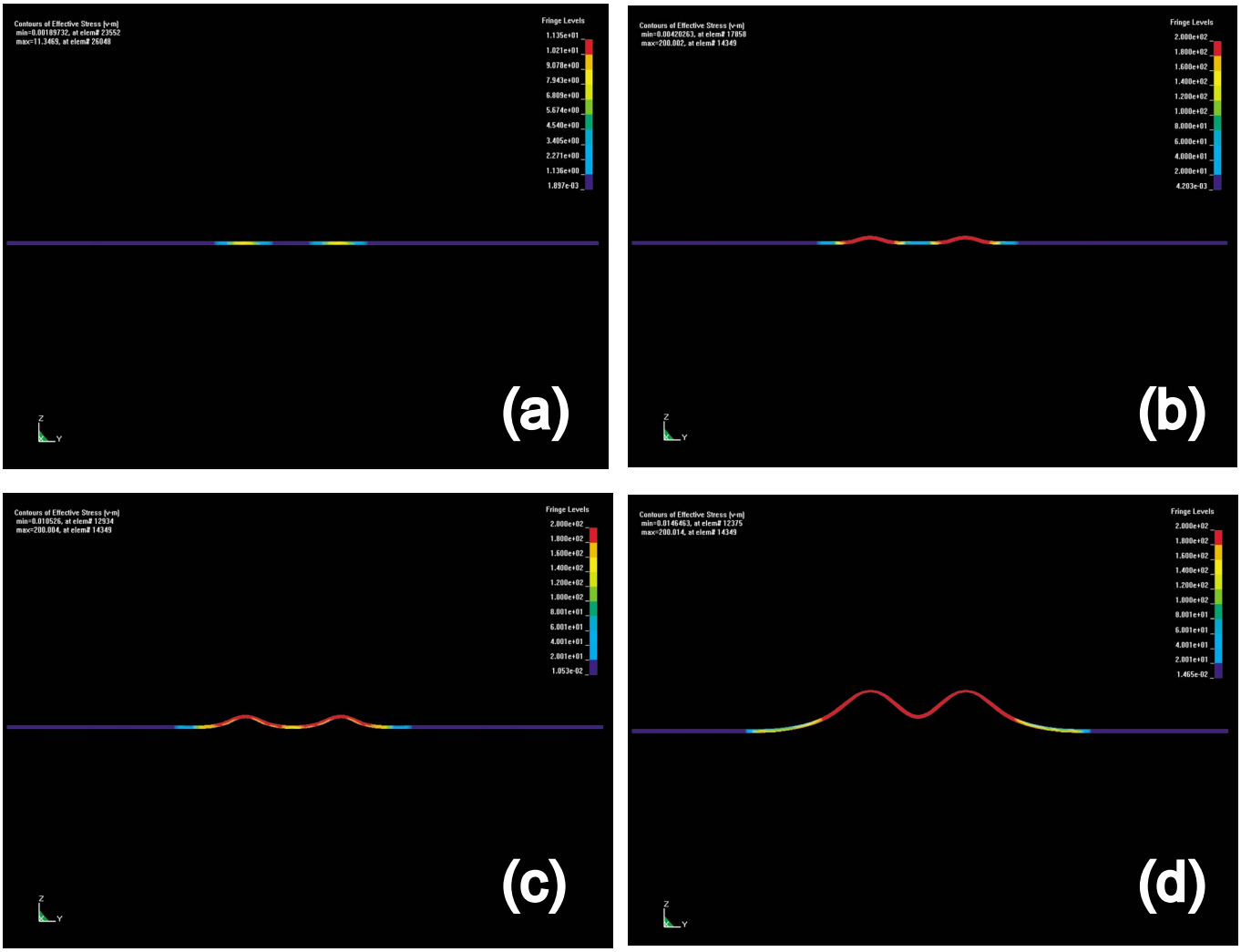

FIG. 4. (Color online) Von-Mises stress distributions in a layer which has two blisters. (a) initial growth of two blisters, (b) stress increment in the middle of two bubbles before merging, (c) merging of bubbles, and (d) splitting of entire domain.

pressures. However, when the pressure is increased and the criterion in Eq. (7) begins to be satisfied, interfacial debonding occurs and coalescence begins. In Fig. 4(c), the nearest neighbor bubbles merge to form a larger bubble and increase in volume. In Fig. 4(d), we are significantly above the delamination criteria, and it can be observed that the entire upper layer exhibits the splitting phenomenon.

In the final stage of bubble growth as shown in Fig. 5, we observe the three dimensional expansion of two debonding areas as two bubble merge to form a single larger bubble. It is interesting to note that the big bubble has an elliptical distribution of Von-Mises stress. The increment in debonded area changes abruptly with pressure above the critical value calculated using Eq. (5) and (6) since the condition described in Eq. (7) applies. With a further increase in pressure, the entire $BaTiO_3$ layer starts to show rigid body motion indicating that the whole layer has been delaminated from the donor substrate.

In conclusion, we show that cavity nucleation and coarsening dominated by the Ostwald ripening mechanism can explain layer delamination in hydrogen implanted ferroelectric single crystal $BaTiO_3$. We propose a simplified debonding criterion derived from the force equilibrium condition using dimensionless parameter extraction. Bond strength was introduced to simulate debonding process. The stress devel-

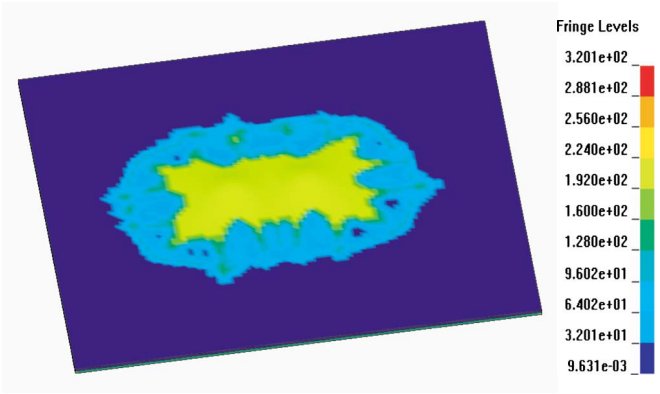

FIG. 5. (Color online) Three-dimensional simulation result for two cavity nucleation and coalescence using Von-Mises stress distribution corresponding to the Fig. 4. Scale bar represents a stress level.

opment during the interaction of two bubbles was investigated through FEM simulation. As expected from experiment, the two bubbles were observed to merge to become a single larger bubble showing an increase in total bubble volume. It should be noted that the material properties of the delaminated layer and the interfacial bond strength after ion implantation damage are of great importance for thin film delamination and therefore for layer transfer processes. In order to induce uniform debonding of an entire thin film domain it is important to avoid rupturing the bubbles as this may cause defects in the layer at the bubble perimeter.

This work has been supported by the Army Research Office (ARO-MURI) under Grant No. DAAD 19-01-1-0517.

*Corresponding author. Electronic address: ypark@caltech.edu

[1] J. F. Ziegler, J. P. Biersack, and U. Littmark, in *The Stopping and Range of Ions in Solid* (Pergamon, New York, 1985).
[2] M. Bruel, Electron. Lett. **31**, 1201 (1995).
[3] Q. Y. Tong, K. Gutjahr, S. Hopfe, U. Goesele, and T. H. Lee, Appl. Phys. Lett. **70**, 1390 (1997).
[4] M. Levy, R. M. Osgood, R. Liu, L. E. Cross, G. S. Cargill, A. Kumer, and H. Bakhru, Appl. Phys. Lett. **73**, 2293 (1998).
[5] I. Szafraniak, I. Radu, R. Scholz, M. Alexe, and U. Gosele, Integr. Ferroelectr. **55**, 983 (2003).
[6] F. J. Kub, K. D. Hobart, J. M. Pond, and S. W. Kirchoefer, Electron. Lett. **35**, 477 (1999).
[7] T. Izuhara, I. Gheorma, R. M. Osgood, A. N. Roy, H. Bakhru, Y. M. Tesfu, and M. E. Reeves, Appl. Phys. Lett. **82**, 616 (2003).
[8] Young-Bae Park, J. L. Ruglovsky, and H. A. Atwater, Appl. Phys. Lett. **85**, 455 (2004).
[9] Q. Y. Tong, K. Gutjahr, S. Hopfe, and U. Gosele, Appl. Phys. Lett. **70**, 1390 (1997).
[10] C. M. Varma, Appl. Phys. Lett. **71**, 3519 (1997).
[11] Q. Y. Tong and U. Gosele, Annu. Rev. Mater. Sci. **28**, 215 (1998).
[12] M. Weldon, M. Collot, Y. Chabal, V. Venezia, A. Agarwal, T. E. Haynes, D. Eaglesham, S. Christman, and E. Chaban, Appl. Phys. Lett. **73**, 3721 (1998).
[13] S. W. Bedell and W. A. Lanford, J. Appl. Phys. **90**, 1138 (2001).
[14] J. W. Huchinson and Z. Sou, Adv. Appl. Mech. **29**, 63 (1992).
[15] M. Georgey, C. Coupeau, J. Colin, F. Cleymand, and J. Grilhe, Philos. Mag. A **82**, 633 (2002).
[16] L. B. Freund, Appl. Phys. Lett. **70**, 3519 (1997).
[17] Young-Bae Park, P. Nardi, X. Li, and H. A. Atwater, J. Appl. Phys. **97**, 074311 (2005).
[18] LS-DYNA user manual, Livermore Software, 2003.
[19] H. K. Birnbaum and P. Sofronis, Mater. Sci. Eng., A **176A**(1/2), 191 (1994).
[20] Y. Fukai, in *The Metal-Hydrogen System: Basic Bulk Properties*, (Springer, Berlin, 1993).
[21] W. Han and J. Yu, J. Appl. Phys. **89**, 6551 (2001).
[22] S. Serebrinsky, E. A. Carter, and M. Ortiz, J. Mech. Phys. Solids **52**, 2403 (2004).
[23] S. Chandrasekhar, Rev. Mod. Phys. **15**, 1 (1943).
[24] V. Raineri, M. Saggio, and E. Rimini, J. Mater. Res. **17**, 1449 (2000).
[25] Y. Wei and J. W. Hutchinson, Int. J. Fract. **93**, 315 (1998).